H_2 Dissociation on Noble Metal Single Atom Catalysts Adsorbed on and Doped into CeO_2 (111)

Journal:	*The Journal of Physical Chemistry*
Manuscript ID	jp-2019-00609z.R1
Manuscript Type:	Article
Date Submitted by the Author:	19-Mar-2019
Complete List of Authors:	Righi, Giulia; Universita degli Studi di Modena e Reggio Emilia, Fisica, Informatica e Matematica; CNR-S3 Institute of Nanoscience Magri, Rita; Universita degli Studi di Modena e Reggio Emilia Dipartimento di Scienze Fisiche Informatiche e Matematiche, Scienze Fisiche, Informatiche e Matematiche; CNR-S3 Institute of Nanoscience Selloni, Annabella; Princeton University, Chemistry

H_2 Dissociation on Noble Metal Single Atom Catalysts Adsorbed on and Doped into CeO_2 (111)

*Giulia Righi[1,2] *, Rita Magri[1,2], Annabella Selloni[3]*

[1] Department of Physics, Informatic, and Mathematic of the University of Modena and Reggio-Emilia

[2] CNR-S3 Institute of Nanoscience, via Campi 213/A, 41100 Modena, Italy

[3]Department of Chemistry, Princeton University, New Jersey, 08540, United States

ABSTRACT:

We used density functional theory (DFT) calculations to investigate the dissociation of H_2 on an Ag single atom catalyst adsorbed on the pristine CeO_2 (111) surface (Ag/CeO_2), or substituting a surface Ce atom on the reduced ($Ag:CeO_{2-x}$) and partially hydrogenated ($Ag:H\text{-}CeO_2$) surfaces. The initial state of the H_2 dissociation reaction in the different investigated models corresponds to distinct oxidation states, +1, +2, or +3, of the Ag atom, thus allowing us to examine the influence of the charge transfers between the noble metal, the oxide and the hydrogen atoms on the reaction pathway and activation energy. In all investigated models, the computed barrier of H_2 dissociation is lowered by about 0.6 eV in comparison to that on metal-free CeO_2. On Ag/CeO_2 and $Ag:CeO_{2-x}$, also the energy of H_2 dissociative adsorption is smaller than on metal-free ceria. These results suggest that CeO_2 modified with dispersed Ag atoms is a promising anode material for proton exchange membrane fuel cells. Further comparison of our results for Ag to analogous calculations for Cu and Au single atom catalysts reveals trends in the computed barriers that can be related to the change of the metal oxidation state in the reaction.

I. Introduction

Catalysts are essential in many industrial and energy conversion processes. Noble metals have shown excellent catalytic properties for energy production and conversion[1], but their use on the large scale is limited by the high cost. An important goal is thus to reduce the amount of noble metal while maintaining or possibly increasing the performance. It was recently proposed that this goal could be achieved by single noble metal atoms on a supporting surface[2]. In this so-called single atom catalysis (SAC), the main catalytic center is an isolated supported metal atom. SAC has received increasing attention over the last years, and new techniques to prepare and characterize single atom catalysts have been developed, including wet chemistry, mass selected soft landing, and atomic layer deposition[1]. While such single atom catalysts are expected to exhibit novel properties in comparison to those of nanoparticle catalysts, understanding of their activity is still limited [3].

In this work, we investigate the reactivity of single noble metal atoms focusing on the dissociation and oxidation of H_2 on Ag, Au and Cu atoms supported on CeO_2 (111), the most stable[4] [5] [6] [7] and frequently exposed surface of CeO_2 nanocrystals. As the reaction occurring at the anodes of proton exchange membrane fuel cells (PEMFCs), the oxidation of H_2 is of both scientific and technological interest. Currently, platinum is the metal of choice for the anode catalyst in PEMFCs but its high cost and scarcity limits its use in industrial applications [8]. Replacing platinum with a cheaper material is crucial for increasing the competitive advantage of fuel cells. A good candidate is cerium oxide, a strongly reducible oxide catalyst[9] [11] [12] that is also known to be a good electrode material for electrochemical devices[10] and to facilitate the oxidation of H_2, especially in the presence of noble or transition metals[13].

As shown by recent experiments, metal atoms on CeO_2 often occupy Ce substitutional sites at low levels of loading[1], and surface cation (Ce) vacancies have been reported to be essential for stabilizing single atom catalysts[1]. Qiao et al. [14] synthesized single Au atom catalysts supported on CeO_2, and observed that the Au atoms were indeed accommodated in the Ce vacancies. Based on the

classification of McFarland et al. [15], Ag, Au, and Cu atoms belong to the class of low valence dopants (LVDs) for CeO_2. The main effect of LVDs is to determine an increase of the oxidative power of the oxygen atoms near the dopant[15]. Consequently, these dopant metal atoms should be good candidates for decreasing the activation energy for H_2 dissociation.

Motivated by the above findings and predictions[1 14], in this work we use first principles calculations to investigate the mechanism of H_2 oxidation on single noble metal atoms either adsorbed on or doped into CeO_2 (111). We mainly focus on single Ag atom catalysts, and compare the adsorption and reactivity of Ag to those of Cu and Au, for which several SAC studies are already available [14 16]. Three different configurations of the single metal atom (M) catalyst are examined: a) M adsorbed on the pristine CeO_2 (111) surface; b) M substituting a Ce atom in the presence of an excess electron supplied by an adsorbed H atom; c) M substituting a Ce atom in the presence of a nearby oxygen vacancy. These configurations correspond to three different initial oxidation states of the noble metal atom, +1 for case a), +3 for case b), and +2 for case c), which allows us to obtain insight into the influence of the metal oxidation state on the activation of H_2. Oxidation states are here evaluated through established procedures based on analysis of geometries, atomic charges and partial densities of states (see Sec. II). Although approximate, this approach is widely used and found to provide meaningful trends for a wide range of systems. While more accurate methods for determining oxidation states are now available[17 18], they are typically quite demanding and outside the scope of the present investigation.

II. Computational Methods

Calculations were performed using spin-polarized density functional theory (DFT) with the gradient-corrected Perdew- Burke-Ernezhof (PBE)[19] exchange and correlation functional as implemented in the Quantum Espresso Package [20 21]. The interaction between electrons and ions was described by ultra-soft pseudopotentials. The wave function and charge density energy cutoffs were set to 30 Ry and 320 Ry, respectively. To account for electron correlations in CeO_2, we applied the Hubbard correction (DFT+U) on the f orbitals of the cerium atoms using the implementation of

Cococcioni et al. [22]. The U parameter was set to 4 eV, a value that reproduces experimental and theoretical results of previous studies.

CeO_2 crystallizes in the fluorite structure. The bulk primitive cell was optimized using a 7 × 7× 7 Monkhorst-Pack (MP) mesh grid [23]; the resulting lattice parameter is a=5.52 Å, in good agreement with the experimental value a_{exp}= 5.41 Å [24]. The CeO_2 (111) surface was modeled using slabs with three O-Ce-O trilayers and 15 Å of vacuum to avoid interactions between the repeated images. A (3×3) surface supercell was used, and the irreducible part of the surface Brillouin zone was sampled using a (2×2×1) MP mesh grid [23]. A (4×4) surface supercell was used to study H_2 dissociation on an Ag_2 dimer. Atomic positions were relaxed with convergence thresholds of 10^{-5} eV and 1×10^{-2} eV/Å for the total energy and ionic forces, respectively. Atoms of the last trilayer were kept fixed in their bulk positions.

The formation energy of an oxygen vacancy was calculated as: $E_{form}=E_{def}+1/2E_{O2}-E_{pristine}$, where E_{def} is the energy of the surface with the oxygen vacancy, $E_{pristine}$ is the energy of the slab without the oxygen vacancy, and E_{O_2} is the energy of the O_2 molecule. The adsorption energy of a noble metal atom on the CeO_2 surface was calculated as $E_{ads}^{M} = E_{M/CeO_2} - E_M - E_{CeO_2}$, where E_{M/CeO_2} is the energy of the surface with the metal absorbed, E_M is the energy of the metal in the gas phase, and E_{CeO_2} is the energy of the pristine surface.The H_2 adsorption energy was calculated as $E_{ads}(H_2) = E_{H_2/M@CeO_2} - E_{H_2} - E_{M@CeO_2}$, where $E_{H_2/M@CeO_2}$ is the energy of the slab with the supported metal atom (M) and the H_2 molecule, $E_{M@CeO_2}$ is the energy of the slab with the supported metal atom but without H_2, and E_{H_2} is the energy of the H_2 molecule. E_{H_2} was determined using a cubic box with a 20 Å edge; the computed bond length is 0.75 Å, in good agreement with the experimental value (0.740 Å) and other DFT calculations (0.743 A [16]).

H_2 dissociation pathways were determined using the climbing image nudged method (CI-NEB) [25] with seven images. Charge transfers along the pathways were estimated by analyzing Bader charges [26] and projected density of states (PDOS).

III. Results and Discussion

III.1. Geometries and Electronic Properties of Single Noble Metal Atom Catalysts on CeO_2(111)

For each single noble metal atom (M), we have studied three different configurations on the CeO_2(111) surface: an adsorbed M (M/CeO_2); M substituting a Ce atom in the presence of an excess electron supplied by an adsorbed H atom (M:H-CeO_2); and M substituting a Ce atom in the presence of a surface oxygen vacancy (M:CeO_{2-x}). Fig. 1 and Fig. S1 show side and top views, respectively, of the three configurations while Fig. 2 reports the corresponding orbital projected density of states (PDOS). For each case, we first discuss the results for Ag and next compare the behavior of Ag to the other noble metals (Cu and Au).

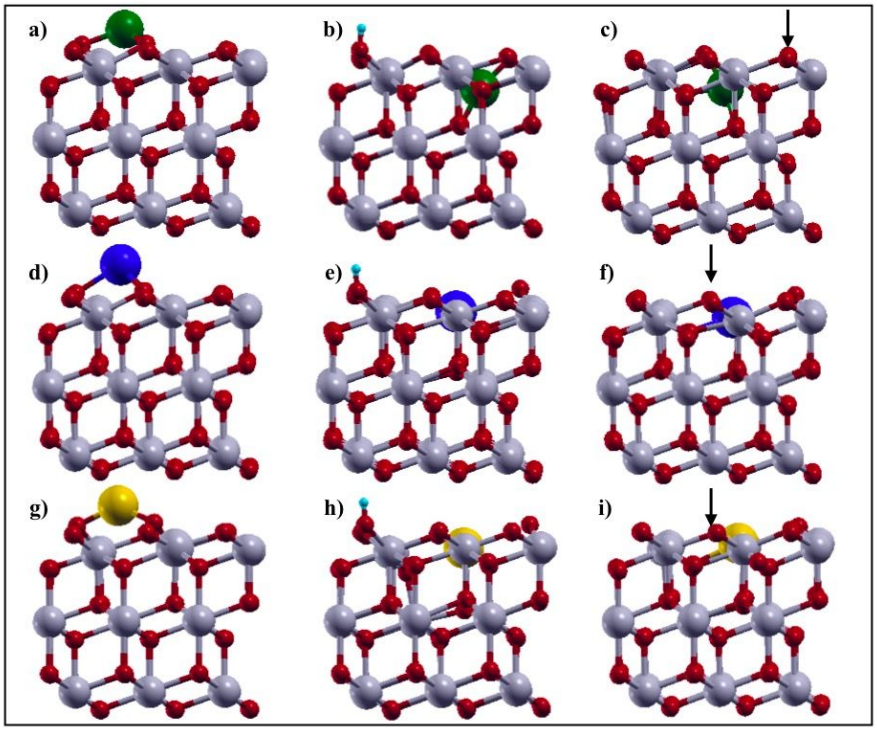

Fig. 1 Models (side views) of a supported noble metal atom M (M = Cu, Ag, Au) on CeO_2(111) investigated in this work: a), d), g) M adsorbed on CeO_2 (M/CeO_2); b), e), h) M substituting a Ce atom in the presence of an adsorbed H (M:H-CeO_2); c), f), i) M substituting a Ce atom in the presence of an Oxygen vacancy (M:CeO_{2-x}). Green (first row), blue (2nd row), and yellow (third row) spheres indicate the Cu, Ag, and Au atoms, respectively. Gray and red balls represent Cerium and Oxygen atoms. Arrows indicate the positions of the Oxygen atoms that were removed. Top views of these models are shown in Figure S1.

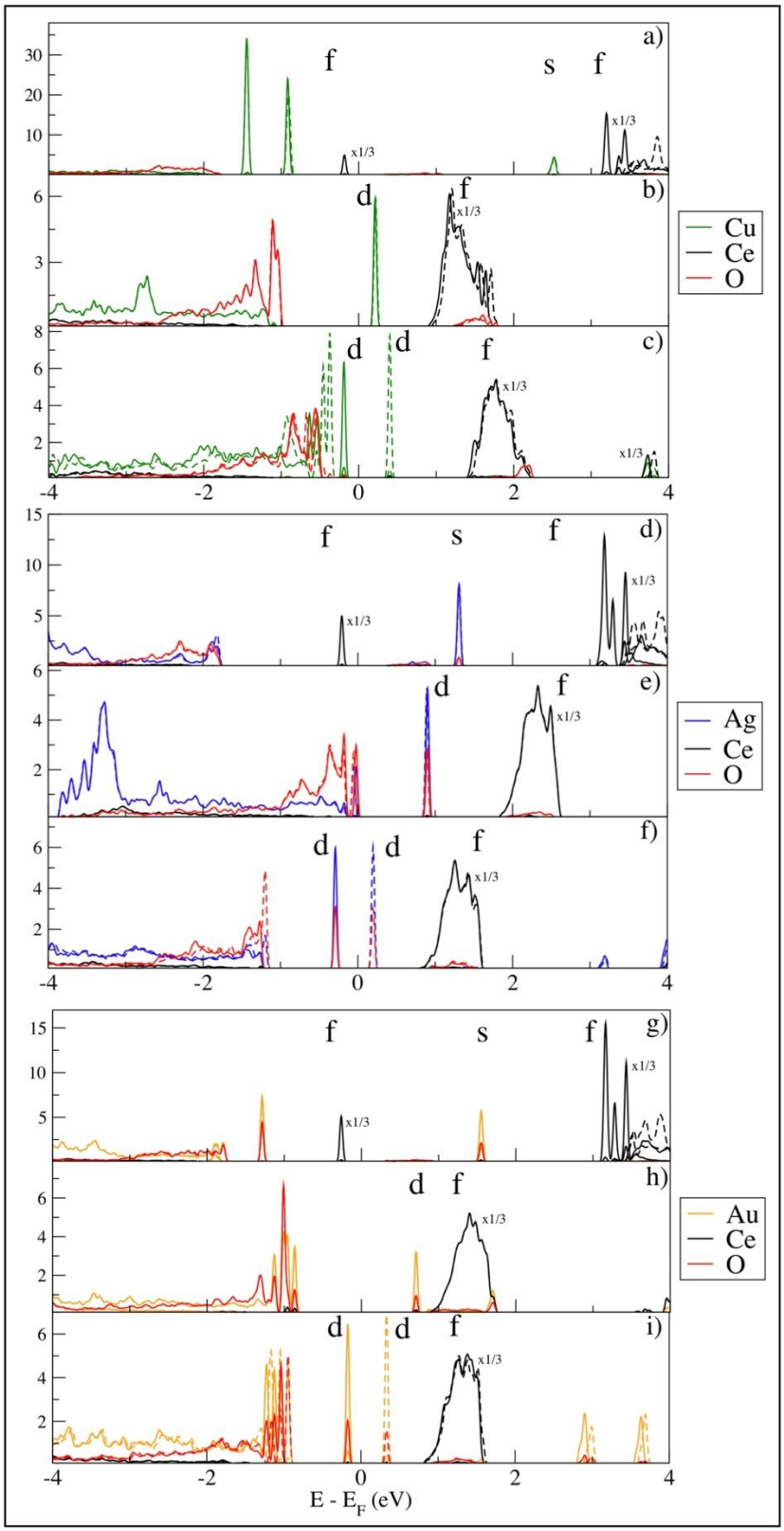

Fig. 2 Projected Density of States of the model systems shown in Fig. 1: a) Cu/ CeO_2; b) Cu:H-CeO_2; c) Cu: CeO_{2-x}; d) Ag/ CeO_2; e) Ag:H-CeO_2; f) Ag: CeO_{2-x} ; g) Au/ CeO_2; h) Au:H-CeO_2; i) Au: CeO_{2-x}. Full and dashed lines refer to spin up and spin down contributions, respectively. f states have been multiplied by a factor 1/3.

III.1.1. *M/CeO₂*

Fig. 1d shows the structure of an adsorbed Ag atom on CeO_2(111). Ag binds on top of an oxygen atom of the third layer and is coordinated to three surface oxygen atoms, with adsorption energy of -1.31 eV. The adsorption causes a charge transfer from Ag to the oxide, which results in the formation of a cation Ag^+, and the reduction of one second neighbor cerium atom from Ce^{4+} to Ce^{3+} (see Fig. S1), as theoretically found also by Tang et al. [27]. Table 1 reports the calculated adsorption energy E_{ads}^{Ag}, the three metal-oxygen bond lengths, the metal – Ce^{3+} bond length, the transferred charge, and the magnetization of the reduced Ce^{3+} ion, resulting from the partial filling of the *f* orbital. In Fig. 2d we show the projected density of states of Ag/CeO_2: the appearance of the Ag *s* peak above the Fermi energy (E_F) and a new Ce f peak below E_F confirms the charge transfer. The new oxidation state of the Ag adatom is +1, with Ag-O distances slightly larger than the experimental values for Ag_2O [28].

The behaviors of Cu and Au are similar to that of Ag. Cu binds on top of a surface oxygen atom of the third layer (Fig. 1d), with a larger adsorption energy (E_{ads}^{Cu}=-2.62 eV) in comparison to Ag, and Cu-O distances slightly larger than those observed in Cu_2O [29]. In contrast to Ag and Cu, Au prefers to adsorb on a bridge site between two surface oxygen atoms, but the adsorption energy difference between the bridge and on top sites is less than 0.10 eV. The Au adsorption energy is E_{ads}^{Au}=-1.12 eV. Similar to Ag, Cu and Au are oxidized to Cu^+ and Au^+ upon adsorption on the CeO_2 surface, and at the same time one Ce atom is reduced to Ce^{3+}. As shown in Fig. 2a and g, the metal *s* peak is indeed empty, and a new Ce *f* peak appears below E_F. The reduced Ce atom is a second neighbor of both Cu [27] and Ag, whereas it is a third neighbor in the case of Au (see Table 1), as found in other computational studies [27 30].

Table 1 Adsorption energy of the metal adatom, in eV, magnetic moment of Ce^{3+} (μ_B), M-O distance (Å) between the metal (M) and neighboring O atoms, M-Ce^{3+} distance (Å) between the metal and the Ce^{3+} ion, charge transfer Δq (e) from the metal adatom to the surface.

M	E_{ads}	μ(Ce^{3+})	M-O	M- Ce^{3+}	Δq
Cu	-2.62	0.89	2.02, 2.03(2)	4.82	0.55
Ag	-1.31	0.89	2.35, 2.41(2)	5.06	0.38
Au	-1.12	0.90	2.15, 2.18	4.71	0.20

III.1.2. *M:H-CeO_2*

The second investigated model is the substitution of a Ce by an Ag atom. Cerium has oxidation state +4 in CeO_2, whereas the highest oxidation state that Ag can have is +3. To compensate for the missing charge, we have introduced an adsorbed H atom on a distant surface oxygen (see Figs. 1 and S1), which provides an additional electron without substantially affecting the interaction of Ag with the H_2 molecule. We found indeed that, in the absence of such a compensating charge, the H_2 molecule tends to react with an oxygen atom of the CeO_2 surface to form an H_2O molecule together with a surface oxygen vacancy, suggesting that the surface needs extra electronic charge to be stabilized. The optimized Ag:H-CeO_2 structure is shown in Fig. 1e. Ag is approximately at the same height of the Ce surface atoms, and the Ag-O bonds are ~ 2.19 Å , slightly larger than those observed in Ag_2O_3[31]. The three oxygen atoms bonded to the Ag metal, and the other oxygen atoms below, show a smaller amount of electronic charge (~ -0.2 e per oxygen atom) than in pure ceria, as found also in a previous computational study for Au [32]. Comparison of the PDOS of Ag:H-CeO_2 (Fig. 2e) and Ag/CeO_2 (Fig. 2d) shows a new Ag peak above E_F for Ag:H-CeO_2, which originates from empty d metal orbitals with some contributions from the *p* states of the less charged oxygen atoms. At the same time, the Bader and Löwdin charges show a depletion of both the *s* and *d* Ag orbitals with respect to the isolated atom. These findings suggest that the new Ag oxidation state is +3, as previously proposed in a theoretical study by Camellone et al. [30] for substitutional Au. This

conclusion is also supported by the Ag - O bond lengths and by the value of the dihedral angle in Ag:H-CeO_2, which is comparable to the dihedral angle in Ag_2O_3 (174.5°). In contrast to the Ag/CeO_2 case, where one reduced Ce^{3+} ion was observed, here all Ce ions have oxidation state +4 (i.e. all *f* states are empty).

The optimized structures of Cu:H-CeO_2 and Au:H-CeO_2 are shown in Fig. 1b and 1h, respectively. Similar to Ag, Au does not introduce major distortions of the surface structure: it remains at the same height of the Ce atoms with Au-O bond lengths of 2.12 Å, in the range of the observed Au-O bond lengths in Au_2O_3 [33]. In contrast, the Cu atom moves down toward a subsurface site with Cu-O bond lengths of 1.89 Å, similar to the observed bond distances in Cu_2O [34]. The PDOS of Cu:H-CeO_2 (Fig. 2b) and Au:H-CeO_2 (Fig. 2h) show metal d states above the Fermi energy, as found for Ag (Fig. 2e). The changes of Cu and Au's Bader charges with respect to the adsorbed atoms are also similar to those found for Ag. All results are consistent with an oxidation state +3 in the case of Au. The picture is less clear for Cu, for which a +2 oxidation state was actually suggested in a computational study by Yang et al. [35].

III.1.3. ***M:CeO$_{2-x}$***

When a surface Ce atom is replaced by Ag, the energy cost to form an oxygen vacancy is found to become negative, -0.69 eV. This implies that O-vacancy formation occurs spontaneously in the presence of substitutional Ag, as computationally predicted by Shapovalov et al. [36]. For comparison, our computed formation energy of a surface oxygen vacancy on metal-free CeO_2(111) surface is 2.05 eV, a value similar to those reported in previous theoretical studies[5] [37]. The configuration generated by removing one of the surface oxygen atoms bonded to the substitutional Ag is shown in Fig. 1f. The excess electrons that result from the creation of the vacancy are acquired by the Ag atom. Analysis of the DOS shows indeed that the spin up empty Ag d state of Ag:H-CeO_2 (Fig. 2e) becomes occupied in Ag:CeO_{2-x} (Fig. 2f), whereas the spin down d state remains empty

(dashed lines). This indicates that the Ag oxidation state is +2 in Ag:CeO_{2-x}. A similar behavior was reported in computational studies by Szabova et al. [38] and Yang et al. [35] for Cu.

In agreement with Yang et al. [35] and Shapovalov et al. [36], our calculations predict that the creation of an oxygen vacancy is thermodynamically favored also in the presence of a substitutional Cu, even though the energy gain (E_{form}= -0.12 eV) is smaller than in the Ag case. In contrast, the creation of an oxygen vacancy is computed to be slightly endothermic, E_{form}=+0.23 eV, in the presence of substitutional Au. Our result is in agreement with the theoretical value obtained by Kim et al. [39], whereas Shapovalov et al. [36] predicted a negative formation energy (-0.36 eV) also in the Au case. The PDOS of Cu:CeO_{2-x} and Au:CeO_{2-x} (Fig. 2c and 2i) are similar to that of Ag:CeO_{2-x}, indicating that both excess electrons from the vacancy are acquired by the noble metal. A different result was reported in a theoretical work by Camellone et al. [30], who found that one of the excess electrons of the oxygen vacancy in Au:CeO_{2-x} is acquired by a Ce atom, leading to a reduced Ce^{3+}.

III.2. Pathways of H_2 dissociation

Recent computational studies of H_2 dissociation on metal-free CeO_2 (111) have predicted an heterolytic mechanism leading to the formation of two adjacent OH and the reduction of two surface Ce^{4+} cations to Ce^{3+} [13 40 41]. Following those studies, we calculated the pathways of H_2 dissociation on all the model systems shown in Fig. 1 using the NEB method [25]. In each case, we considered an initial state (IS) where the H_2 molecule is physically adsorbed on the surface and a final state (denoted FS_{NEB}) where the molecule is dissociated. For the IS, we always examined several possible configurations of H_2 on the relaxed surface and chose the one energetically most stable. Considering that H_2 dissociation is likely to occur at the metal site, for the FS_{NEB} we chose a configuration with one H atom of H_2 bonded to the noble metal atom and the other bonded to a surface oxygen atom, rather than the most stable configuration (denoted FS) with both H atoms adsorbed on surface oxygen atoms. FS_{NEB} was found however to evolve spontaneously to FS in the case M:H-CeO_2.

For better clarity, in the following we will report two reaction energies: the first one, ΔE_{NEB}, is the energy difference between the final and initial states of the NEB calculation; the other, ΔE, is the energy of the "true" (most stable) final state with the two H atoms on surface oxygen atoms, referred to the non-interacting gas phase H_2 molecule and M-CeO_2 system.

III.2.1. *H_2 dissociation on Ag/CeO_2*

The minimum energy pathway (MEP) for H_2 dissociation on Ag/CeO_2(111) is shown in Fig. 3. In the IS, the H_2 molecule is weakly adsorbed on the Ag adatom, with a binding energy of 0.27 eV. The H_2 bond length is 0.80 Å (vs 0.75 Å in the gas phase) and the Ag-H distance is 1.91 Å. The PDOS shows no charge transfer from H_2 to the surface (Fig. 4a IS). As final state FS_{NEB}, we consider a configuration with one H bonded to Ag (bond length ~1.62 Å), the other bonded to a surface oxygen O_s (bond length ~ 0.99 Å), and the Ag adatom bonded to only one surface oxygen (bond length ~ 2.15 Å). The H atom adsorbed onto O_s transfers its electron to a surface Ce atom reducing it to Ce^{3+}, while the other H reduces the Ag adatom from Ag^+ to Ag^0, as shown by the PDOS in the bottom panel of Fig. 4a, where the Ag s peak is below the Fermi energy. From the MEP in Fig. 3, we can also see that in the initial stages of the reaction the Ag atom rotates towards O_s, and breaks one of its O-Ag bonds. At the transition state (TS), the bond length of the H_2 molecule has increased to 0.90 Å, and one H atom forms a hydrogen bond with O_s (dashed line in Fig. 3), with a O_s–H bond length of 1.64 Å, while the other H remains bonded to the Ag atom. The Ag s orbital remains empty and a Ce^{3+} peak is still present in the PDOS (Fig. 4a, TS). This TS is only 0.23 eV higher in energy than the IS. We have also determined the barrier for H transfer from Ag (FS_{NEB}) to a near surface Oxygen (FS), and found it to be 1.0 eV. This barrier is quite high in comparison to that for H_2 dissociation, suggesting that FS_{NEB} is an observable intermediate of the reaction.

To test the dependence of the activation and reaction energies on the Hubbard U value[42], we have further calculated the MEP of H_2 dissociation on Ag/CeO_2 using a Hubbard U parameter U=4.5 eV, a value employed by several other authors [13 40 41]. As shown in Fig. S2, the variation of the activation energy is negligible: E_a= 0.22 eV instead of 0.23 eV obtained with U=4 eV.

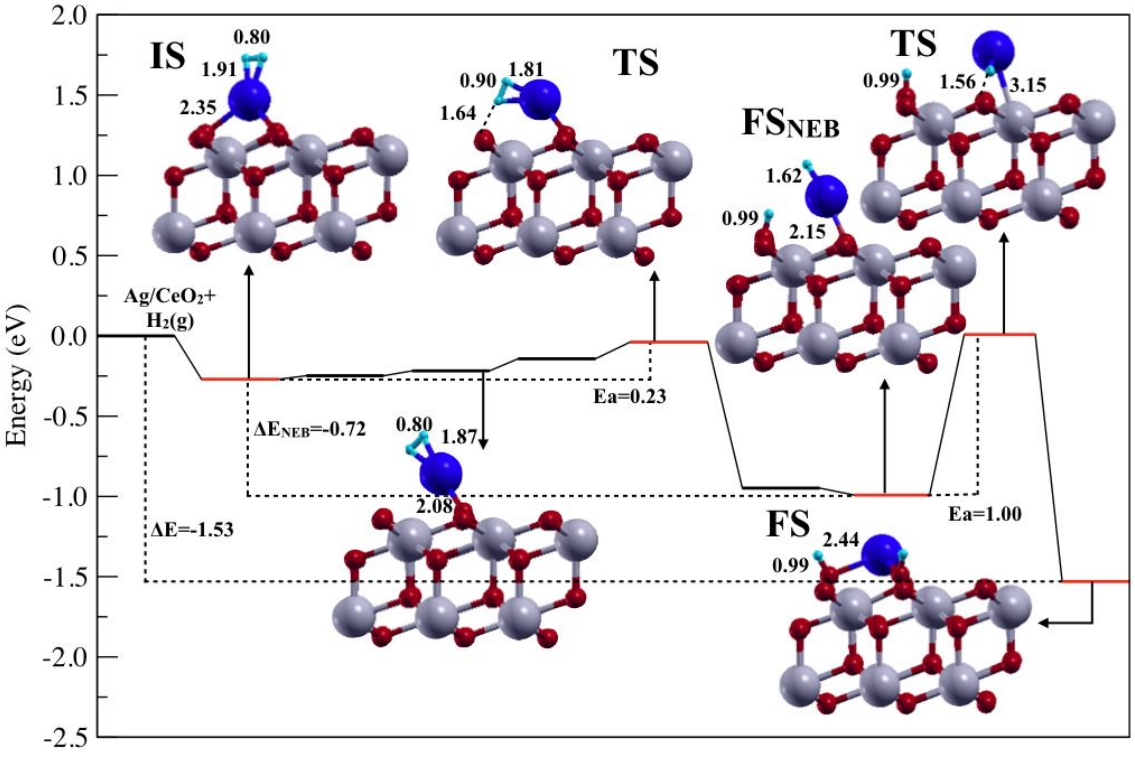

Fig. 3 Potential energy profile along the Minimum Energy Pathway (MEP) of H_2 dissociation on Ag/CeO_2 (111), as obtained by CI-NEB calculations with seven images. Relevant distances are reported. Light blue, blue, gray, and red balls represent the Hydrogen, Silver, Cerium, and Oxygen atoms, respectively. All the distances are in Angstrom.

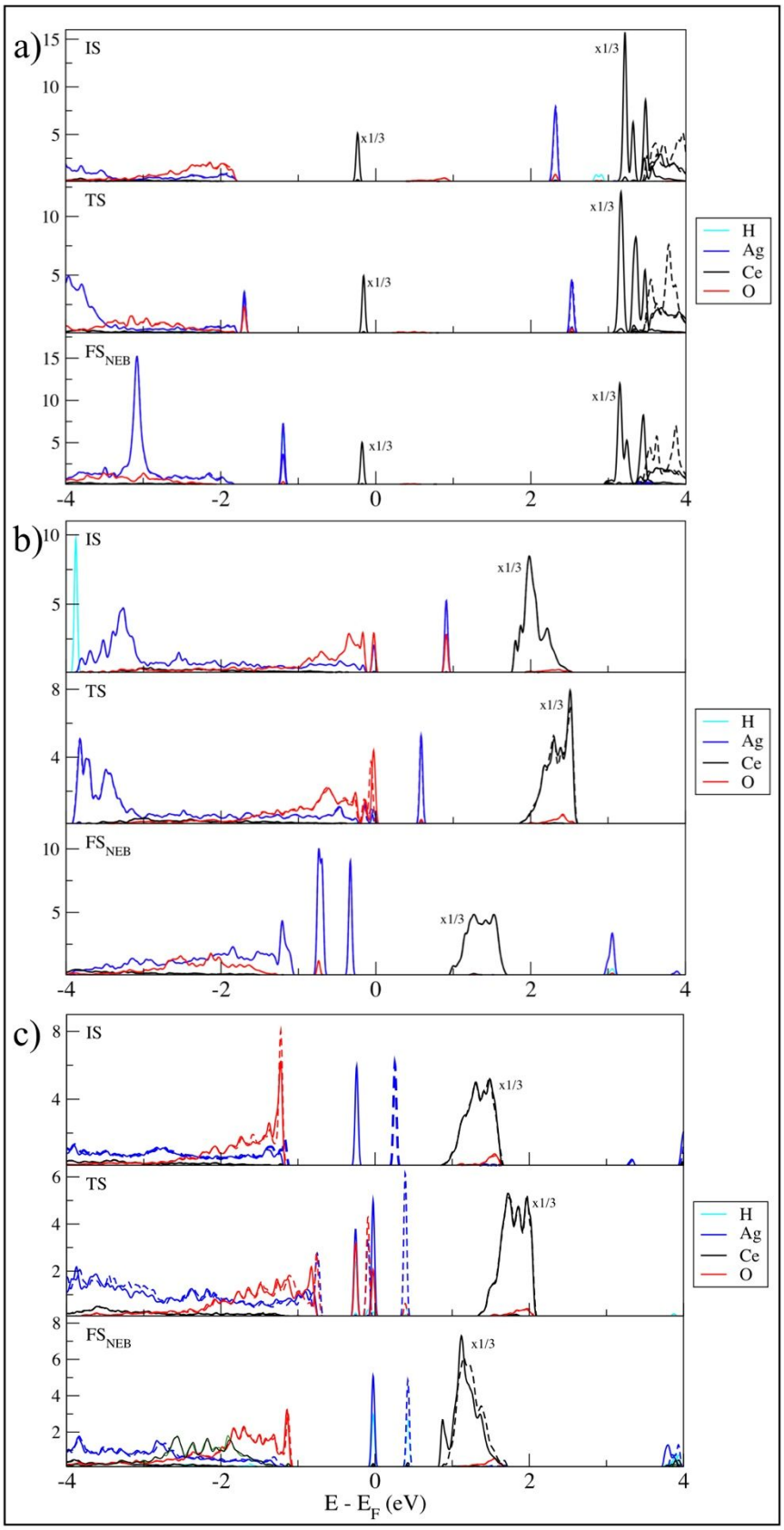

Fig. 4. Projected Density of States for the IS, TS, and FS_{NEB} of H_2 dissociation on: a) Ag/CeO_2; b) $Ag:H-CeO_2$; c) $Ag:CeO_{2-x}$. Full and dashed lines represent the spin up and spin down contributions, respectively.

Similar mechanisms of H_2 dissociation are found on Cu/CeO_2 and Au/CeO_2, see Figs. S3, S4, S5 and S6 of the Supporting Information (SI). In the IS, H_2 is adsorbed on the metal atom with adsorption energies of -0.35 and -0.93 eV, for Cu and Au, respectively, and the molecule is more stretched than in the Ag case. On Au/CeO_2, the Au atom shifts from the bridge to the on-top site upon H_2 adsorption; a similar change of metal adsorption site was observed also in a theoretical study of CO oxidation on Au/CeO_2 by Camellone et al. [30]. The existence of a bond between Au and H was assumed also by Jaurez et al. [43] to explain their experimental results on H_2 dissociation on Au/CeO_2.

The activation energy (E_a) and reaction energies (ΔE_{NEB} and ΔE) of H_2 dissociation on the three M/CeO_2 surfaces are compared in Table 2, which shows also results for metal-free ceria from previous DFT studies. The presence of the noble metal atom on the CeO_2 surface decreases the barrier of H_2 dissociation (from 0.99 eV to ~ 0.30 eV) and at the same time makes the reaction energy less negative, indicating that a single noble metal atom adsorbed on the CeO_2 (111) is an efficient catalyst for H_2 dissociation. The charge transfer from the metal adatom to the CeO_2 surface is crucial in favoring the initial binding of the H_2 molecule to the catalyst. This initial binding facilitates the dissociation with respect to the case of pure ceria where H_2 does not bind to the surface. The smaller absolute value of ΔE on M/CeO_2 relative to pure CeO_2 indicates that the H atoms are less strongly bound to the surface, which should facilitate the subsequent proton release during PEMFC operation.

Table 2 Activation energies (E_a) and reaction energies (ΔE_{NEB} and ΔE) for H_2 dissociation on pure CeO_2 (from previous computational studies, as indicated), Cu/CeO_2, Ag/CeO_2, and Au/CeO_2 (from this work). ΔE_{NEB} is the energy difference between the final and initial states of the NEB calculation, whereas ΔE is the

energy of the H_2 dissociated state with both H atoms on surface oxygens relative to the non-interacting H_2 molecule and M/CeO_2 surface. All energies in eV.

	CeO_2	Cu	Ag	Au
E_a	0.99 [13] 0.99 [41] 1.08 [40]	0.29	0.23	0.35
ΔE_{NEB}	-2.50 [13] -2.34 [41] -2.50 [40]	-0.55	-0.72	-1.27
ΔE	-2.50 [13] -2.34 [41] -2.50 [40]	-1.99	-1.53	-2.32

III.2.2. *H_2 dissociation on Ag:H-CeO_2*

The MEP for H_2 dissociation on Ag-doped CeO_2 in the presence of an adsorbed H is shown in Fig. 5. In the initial state, H_2 is physically adsorbed (E_{ads}= -0.03 eV) with one of its H atoms at distance ~ 2.75 Å from a surface oxygen, and the Ag oxidation state is +3 (Fig. 4b IS). As H_2 moves towards the surface, one of the Ag-O bonds with the surface breaks. At the TS, the H_2 molecule (bond length ~ 0.80 Å) is adsorbed on the Ag atom (Ag-H distance ~ 2.15 Å) while forming also a H-bond with a surface O atom (O_s) at distance ~ 1.80 Å. From the PDOS it appears that the Ag oxidation state is still +3 at the TS (Fig. 4b TS). After the H-H bond breaks, one hydrogen atom moves directly to O_s while the other moves spontaneously from Ag to another nearby surface oxygen atom. The activation energy for dissociation, E_a = 0.33 eV, is significantly lower than in pure CeO_2. In this system the final state FS_{NEB} transforms spontaneously to (i.e. coincides with) FS, H_2 is dissociated with both H atoms adsorbed on surface oxygen atoms and Ag is reduced. As shown by the PDOS in the bottom panel of Fig. 4b, the Ag d states are indeed below E_F, while the CeO_2 surface remains oxidized, indicating that the Ag oxidation state is +1.

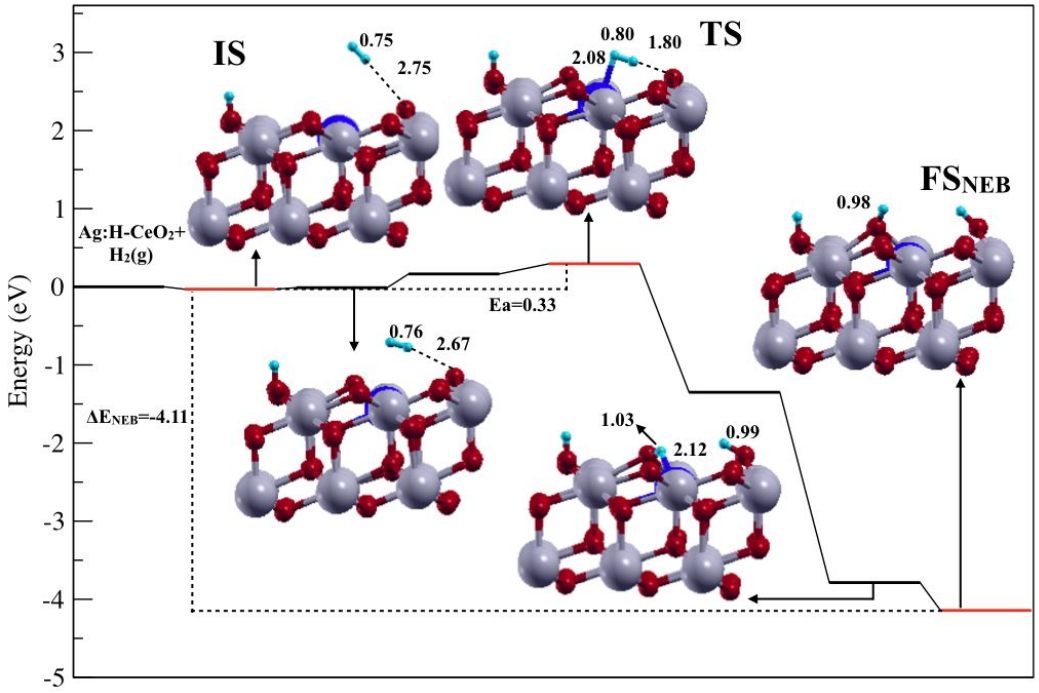

Fig. 5 Potential energy profile along the MEP of H_2 dissociation on Ag:H-CeO_2(111). Relevant distances (in Å) are reported. The color code is the same as in Fig. 3.

The analogous pathways on Cu:H-CeO_2 and Au:H-CeO_2 are qualitatively similar to those for Ag:H-CeO_2 (Figs. S7 and S8), but the charge transfers upon H_2 dissociation are different. In the Au case, the electrons of both H atoms are transferred not to the noble metal but to the surface, leading to the reduction of two Ce cations from Ce^{4+} to Ce^{3+}, while Au maintains an oxidation state +3 (Fig. S4b). On Cu:H-CeO_2, Cu is reduced to an oxidation state +2 after H_2 dissociation, as indicated by the PDOS in Fig. S3b.

In Table 3 we compare the activation and reaction energies of H_2 dissociation on Ag, Au and Cu doped CeO_2 (M:H-CeO_2). Both the activation and reaction energies are much lower on the metal doped surfaces than on pristine CeO_2 (111), and the decrease is more significant for Ag than for Au and Cu.

Charge transfers appear to have a key role in the reaction: Ag facilitates the dissociation of H_2 by becoming reduced from Ag^{3+} to Ag^{+}, its preferred oxidation state, whereas Au is already in its favorite oxidation state (+3) in the IS, so that its effect on H_2 dissociation is less pronounced. On the other

hand, the strong stability of the final state of H_2 dissociation on M:H-CeO_2, especially in the Ag case, implies that it is difficult to break the bonds of the adsorbed H atoms with the surface and regenerate the catalyst as required in PEMFCs.

Table 3 Activation energies (E_a) and reaction energies (ΔE_{NEB} and ΔE) of H_2 dissociation on noble metal doped CeO_2 in the presence of adsorbed H (M:H-CeO_2) or an oxygen vacancy (M:CeO_{2-x}). ΔE_{NEB} is the energy difference between the final and initial states of the NEB calculation, while ΔE is the energy of the H_2 dissociated state with both H atoms on surface oxygens relative to the non-interacting gas-phase H_2 molecule and doped surface. All energies in eV.

	M:H-CeO_2			M:CeO_{2-x}		
	Cu	Ag	Au	Cu	Ag	Au
E_a	0.51	0.33	0.62	0.80	0.34	0.19
ΔE_{NEB}	-2.36	-4.11	-3.00	-0.55	-0.89	-1.43
ΔE	-2.37	-4.14	-3.03	-2.13	-2.83	-2.89

III.2.3. *H_2 dissociation on Ag:CeO_{2-x}*

As discussed in Sec. III.1.3, the substitution of a Ce atom by a noble metal favors the formation of oxygen vacancies, so that M:CeO_{2-x} is the actual stable configuration of M-doped CeO_2. The pathway and activation energy for H_2 dissociation on Ag:CeO_{2-x} (Fig. 6 and Table 3) are similar to those on Ag:H-CeO_2 (Fig. 5). The initial Ag oxidation state on Ag:CeO_{2-x} is +2 (Fig. 4c, IS), and the PDOS changes after H_2 dissociation (Fig. 4c, FS_{NEB}) suggest partial transfer of the hydrogen electrons to both Ag and the CeO_2 surface. This is confirmed by the Bader and Löwdin charges, which show an increase of the occupation of the Ag *s* orbital with respect to the IS. However, a clear Ag oxidation state of +1 is observed only after both H atoms are bonded to surface Oxygen atoms. The computed barrier for H diffusion from Ag to a surface Oxygen atom is 0.16 eV, a value significantly lower than the activation energy, 0.34 eV, of H_2 dissociation.

The activation and reaction energies of H_2 dissociation on Cu:CeO_{2-x} and Au:CeO_{2-x} are summarized in Table 3, while pathways and PDOS are reported in Figs. S9-S10 and S5-S6,

respectively. The barrier is low (0.19 eV) on Au:CeO_{2-x}, whereas it is quite high (0.80 eV) on Cu:CeO_{2-x}. A possible reason of this difference is that the initial +2 oxidation state is very stable for Cu whereas it is not as favorable for Ag and Au, which prefer to take an oxidation state +1, hence facilitating the dissociation of the H_2 molecule. On the other hand, the smaller H_2 dissociation barrier on Au:CeO_{2-x} in comparison to Ag:CeO_{2-x} may be related to the different TS geometries: on Au:CeO_{2-x} the H_2 bond at the TS is only slightly longer than at equilibrium (0.78 Å), whereas on Ag:CeO_{2-x} the H-H bond at the TS is stretched to 0.91 Å, thus requiring more energy.

The low value of E_a predicted by our calculations for Au:CeO_{2-x} appears to disagree with a recent study by Qiao et al. [14] showing that atomically dispersed Au on CeO_2 does not activate H_2 at temperatures below 100 C. On the other hand, our value E_a = 0.62 eV for H_2 dissociation on H-Au:CeO_2 is both consistent with the experimental observation by Qiao et al. [14] and also agrees with their computed activation barrier of 0.69 eV for H_2 dissociation on atomically dispersed Au atoms at Ce sites (with no oxygen vacancy). Therefore, a possible explanation for the discrepancy of our results for Au:CeO_{2-x} with experiment[14] is the excessive reduction of the Au:CeO_{2-x} model, as suggested also by the positive value of the corresponding O-vacancy formation energy in Sec. III.1.3.

Table 3 also shows that the reaction energies ΔE are in absolute value smaller on M:CeO_{2-x} than on M:H-CeO_2, suggesting that the presence of oxygen vacancies improves the activity of noble metal doped CeO_2 as anode material for PEMFCs.

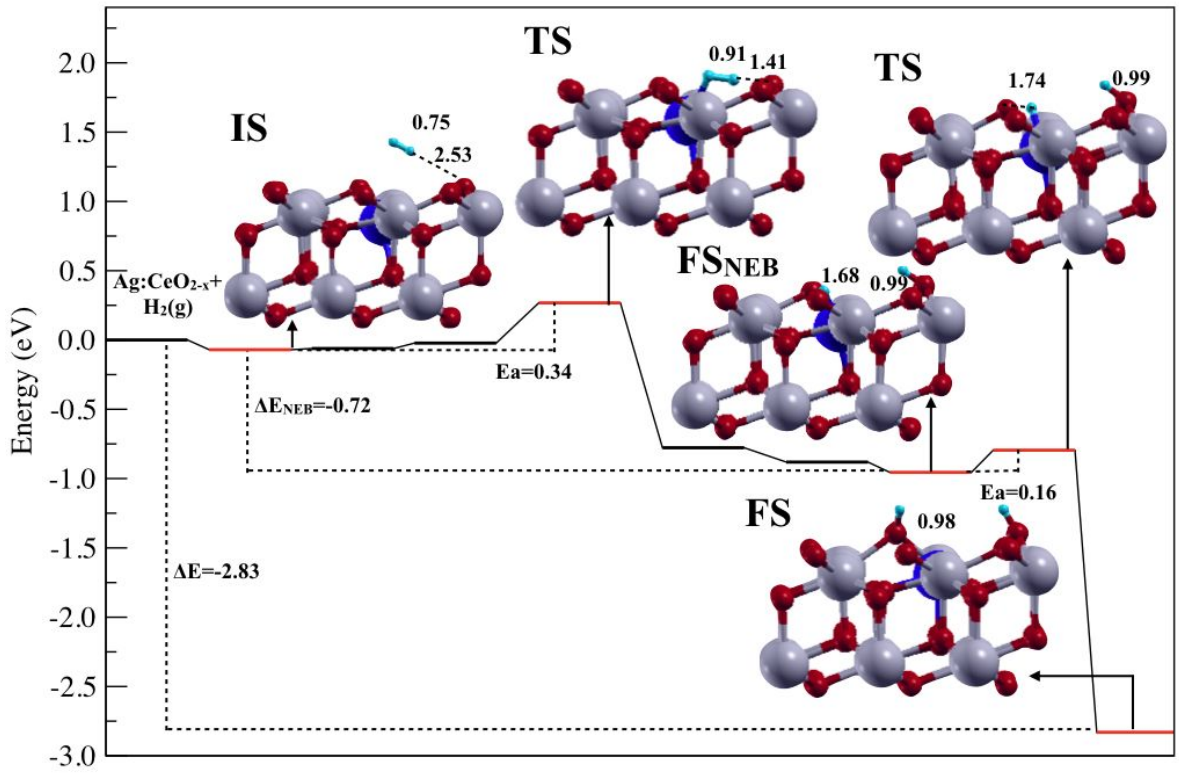

Fig. 6. Potential energy profile along the MEP of H_2 dissociation on Ag:CeO_{2-x} (111), as obtained by CI-NEB calculations with seven images. The color code is the same as in Fig. 3. All the distances are in Angstrom.

III.2.4. *H_2 dissociation on Ag_2*

The results in the previous sections show that the presence of a single adsorbed or substitutional noble metal atom on the CeO_2 surface facilitates the dissociation of H_2. However, it is experimentally difficult to synthesize dispersed single atoms on a supporting surface. We have studied the behavior of an Ag adatom on the doped Ag:CeO_{2-x} surface and found that it is indeed energetically favorable for the adatom to bind to the Ag dopant. The resulting Ag-Ag dimer has a bond distance of 2.75 Å, slightly larger than the calculated bond length of an Ag_2 dimer in the gas phase.

The computed H_2 dissociation pathway on the supported Ag dimer is shown in Fig. 7. Initially the hydrogen molecule is physically adsorbed (IS), whereas in the final state of the NEB calculation one H atom is bonded to a surface oxygen, and the other to the Ag adatom. Along the MEP, H_2 approaches the surface, until it binds to the adsorbed Ag atom (TS) with a H-H bond length of 0.80 Å. Upon

dissociation, one H atom moves onto the surface oxygen to which it was H-bonded while the other stays on the Ag atom. The activation energy of the process, only 0.12 eV, is significantly lower than on pure ceria, as well as on Ag:H-CeO_2 and Ag:CeO_{2-x}.

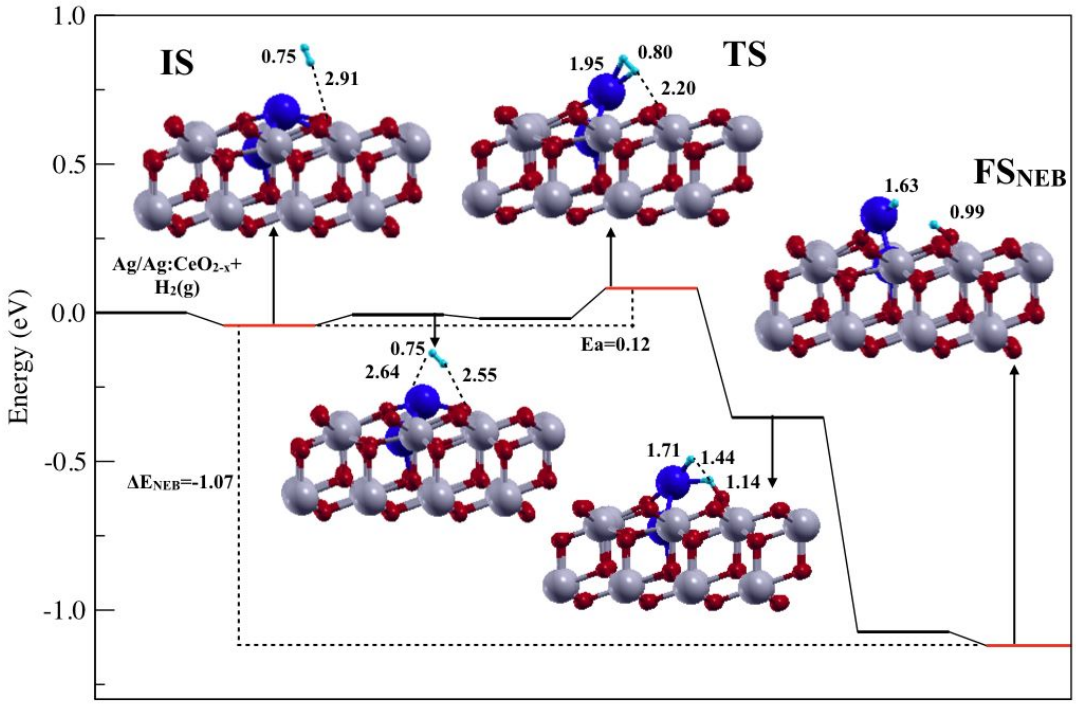

Fig. 7. Potential energy profile along the Minimum energy Pathway (MEP) of H_2 dissociation on Ag on Ag:CeO_{2-x}(111) as obtained by CI-NEB calculations with seven images. The color code is the same as in Figure 3. Reported distances are in Angstrom.

CONCLUSIONS

In this work, we have used ab-initio calculations to investigate the mechanism of H_2 dissociation on single Ag, Au and Cu atoms deposited on or doped into CeO_2 (111). An important goal has been to identify an efficient hydrogen oxidation catalyst that might possibly replace Pt as anode material for PEMFCs. We have focused mainly on Ag, whose activity toward H_2 dissociation has been explored for the first time in this work, and considered different surface models, which has allowed us to investigate the effect of different initial oxidation states of the noble metal atom on the activation of H_2. Our results show that noble metal atoms generally induce a significant decrease of the H_2

dissociation barrier with respect to the pure ceria surface, and the charge transfers involved in the reaction play a crucial role in this decrease. For noble metal adatoms on pristine ceria (M/CeO_2), the initial metal oxidation state is +1 and the charge transfers involved in H_2 dissociation are the same for all metals. Ag/CeO_2 shows the lowest activation energy as well as the less negative reaction energy among the different supported metals (see Table 2), which makes it a potentially interesting material for PEMFC anodes. In the case where the noble metal is substitutional to a surface Ce atom, the formation of oxygen vacancies is highly favored ($M:CeO_{2-x}$). The initial metal oxidation state is +2, and among the different metals Au has the lowest activation energy, closely followed by Ag, which also shows a slightly less negative reaction energy (Table 3). Finally, as an alternative to the formation of an oxygen vacancy, we also considered the case where the missing charge of the substitutional noble metal atom is partially compensated by an adsorbed H ($M:H\text{-}CeO_2$). In this case the initial metal oxidation state is +3 and Ag induces the largest decrease of the activation energy with respect to pure ceria (Table 3). Ag plays an active role by acquiring the electrons of the dissociated H_2 molecule, so that its oxidation state changes from +3 to +1, which is the optimal one for Ag.

In general, we found that when the noble metal atom is in its favored oxidation state in the initial state of the reaction, the energy barrier lowering with respect to pure ceria is small: this is the case of H_2 dissociation on $Au:H\text{-}CeO_2$ or $Cu:CeO_{2-x}$. Except for these cases, the noble metal participates actively in the reaction and contributes to the barrier lowering by accepting electrons from H_2 so as to reach its favorite oxidation state. Finally, our results indicate that CeO_2 modified with single Ag atoms is a promising candidate material for replacing Platinum in the anode of PEMFCs.

ASSOCIATED CONTENT

Supporting Information

Top view of the different configurations (Fig. S1), potential energy profile of H_2 dissociation for Ag/CeO_2 using U=4.5 eV (Fig. S2) , potential energy profile of H_2 dissociation for Cu/CeO_2 and Au/CeO_2 (Fig. S3 and S4), projected density of states (Fig. S5 and S6), potential energy profile of

H_2 dissociation for Cu:H-CeO_2 and Au:H-CeO_2 (Fig. S7 and S8), potential energy profile of H_2 dissociation for Cu:CeO_{2-x} and Au:CeO_{2-x} (Fig. S9 and S10).

AUTHOR INFORMATION

Corresponding Author

* E-mail: giulia.righi@unimore.it

ACKNOWLEDGEMENTS

This work was supported by DoE-BES, Division of Chemical Sciences, Geosciences and Biosciences under Award DE-SC0007347. We acknowledge use of the computational resources of TIGRESS high performance computer center at Princeton University. We thank the University of Modena and Reggio Emilia for financial support through the Bando Mobilità Giovani Ricercatori and the project FAR 2016.

REFERENCES

(1) Liu, J. Catalysis by Supported Single Metal Atoms. *Acs Catalysis* **2016**, *7* (1), 34–59.
(2) Chen, Y.; Huang, Z.; Ma, Z.; Chen, J.; Tang, X. Fabrication{,} Characterization{,} and Stability of Supported Single-Atom Catalysts. *Catal. Sci. Technol.* **2017**, *7* (19), 4250–4258. https://doi.org/10.1039/C7CY00723J.
(3) Fako, E.; Łodziana, Z.; López, N. Comparative Single Atom Heterogeneous Catalysts (SAHCs) on Different Platforms: A Theoretical Approach. *Catalysis Science & Technology* **2017**, *7* (19), 4285–4293.
(4) Skorodumova, N. V; Baudin, M.; Hermansson, K. Surface Properties of CeO 2 from First Principles. *Physical Review B* **2004**, *69* (7), 75401.
(5) Fabris, S.; Vicario, G.; Balducci, G.; de Gironcoli, S.; Baroni, S. Electronic and Atomistic Structures of Clean and Reduced Ceria Surfaces. *The Journal of Physical Chemistry B* **2005**, *109* (48), 22860–22867.
(6) Mullins, D. R.; Overbury, S. H.; Huntley, D. R. Electron Spectroscopy of Single Crystal and Polycrystalline Cerium Oxide Surfaces. *Surface Science* **1998**, *409* (2), 307–319.
(7) Siegel, D. A.; Chueh, W. C.; El Gabaly, F.; McCarty, K. F.; de la Figuera, J.; Blanco-Rey, M. Determination of the Surface Structure of CeO2 (111) by Low-Energy Electron Diffraction. *The Journal of chemical physics* **2013**, *139* (11), 114703.
(8) Lykhach, Y.; Bruix, A.; Fabris, S.; Potin, V.; Matol\'\inová, I.; Matol\'\in, V.; Libuda, J.; Neyman, K. M. Oxide-Based Nanomaterials for Fuel Cell Catalysis: The Interplay between Supported Single Pt Atoms and Particles. *Catalysis Science & Technology* **2017**, *7* (19), 4315–4345.
(9) Andersson, D. A.; Simak, S. I.; Johansson, B.; Abrikosov, I. A.; Skorodumova, N. V. Modeling of Ce O 2, Ce 2 O 3, and Ce O 2- x in the LDA+ U Formalism. *Physical Review B* **2007**,

75 (3), 35109.
(10) Tsipis, E. V; Kharton, V. V. Electrode Materials and Reaction Mechanisms in Solid Oxide Fuel Cells: A Brief Review. *Journal of Solid State Electrochemistry* **2008**, *12* (11), 1367–1391.
(11) Montini, T.; Melchionna, M.; Monai, M.; Fornasiero, P. Fundamentals and Catalytic Applications of CeO2-Based Materials. *Chemical Reviews* **2016**, *116* (10), 5987–6041. https://doi.org/10.1021/acs.chemrev.5b00603.
(12) Paier, J.; Penschke, C.; Sauer, J. Oxygen Defects and Surface Chemistry of Ceria: Quantum Chemical Studies Compared to Experiment. *Chemical Reviews* **2013**, *113* (6), 3949–3985. https://doi.org/10.1021/cr3004949.
(13) Negreiros, F. R.; Camellone, M. F.; Fabris, S. Effects of Thermal Fluctuations on the Hydroxylation and Reduction of Ceria Surfaces by Molecular H2. *The Journal of Physical Chemistry C* **2015**, *119* (37), 21567–21573.
(14) Qiao, B.; Liu, J.; Wang, Y.-G.; Lin, Q.; Liu, X.; Wang, A.; Li, J.; Zhang, T.; Liu, J. Highly Efficient Catalysis of Preferential Oxidation of CO in H2-Rich Stream by Gold Single-Atom Catalysts. *ACS Catalysis* **2015**, *5* (11), 6249–6254.
(15) McFarland, E. W.; Metiu, H. Catalysis by Doped Oxides. *Chemical reviews* **2013**, *113* (6), 4391–4427.
(16) Wang, S.; Zheng, M.; Li, M.; Wu, X.; Xia, C. Synergistic Effects towards H2 Oxidation on the Cu–CeO2 Electrode: A Combination Study with DFT Calculations and Experiments. *J. Mater. Chem. A* **2016**, *4* (15), 5745–5754. https://doi.org/10.1039/C6TA00732E.
(17) Ao, B.; Qiu, R.; Hu, S.-X. First-Principles Insights into the Oxidation States and Electronic Structures of Ceria-Based Binary, Ternary, and Quaternary Oxides. *The Journal of Physical Chemistry C* **2019**, *123* (1), 175–184. https://doi.org/10.1021/acs.jpcc.8b09852.
(18) Walsh, A.; Sokol, A. A.; Buckeridge, J.; Scanlon, D. O.; Catlow, C. R. A. Oxidation States and Ionicity. *Nature Materials* **2018**, *17* (11), 958–964. https://doi.org/10.1038/s41563-018-0165-7.
(19) Perdew, J. P.; Burke, K.; Ernzerhof, M. Generalized Gradient Approximation Made Simple [Phys. Rev. Lett. 77, 3865 (1996)]. *Phys. Rev. Lett.* **1997**, *78* (7), 1396. https://doi.org/10.1103/PhysRevLett.78.1396.
(20) Giannozzi, P.; Baroni, S.; Bonini, N.; Calandra, M.; Car, R.; Cavazzoni, C.; Ceresoli, D.; Chiarotti, G. L.; Cococcioni, M.; Dabo, I.; et al. QUANTUM ESPRESSO: A Modular and Open-Source Software Project for Quantum Simulations of Materials. *Journal of physics: Condensed matter* **2009**, *21* (39), 395502.
(21) Giannozzi, P.; Andreussi, O.; Brumme, T.; Bunau, O.; Nardelli, M. B.; Calandra, M.; Car, R.; Cavazzoni, C.; Ceresoli, D.; Cococcioni, M.; et al. Advanced Capabilities for Materials Modelling with QUANTUM ESPRESSO. *Journal of Physics: Condensed Matter* **2017**, *29* (46), 465901.
(22) Cococcioni, M.; de Gironcoli, S. Linear Response Approach to the Calculation of the Effective Interaction Parameters in the $\mathrm{LDA}+\mathrm{U}$ Method. *Phys. Rev. B* **2005**, *71* (3), 35105. https://doi.org/10.1103/PhysRevB.71.035105.
(23) Monkhorst, H. J.; Pack, J. D. Special Points for Brillouin-Zone Integrations. *Phys. Rev. B* **1976**, *13* (12), 5188–5192. https://doi.org/10.1103/PhysRevB.13.5188.
(24) Eyring, L. *Handbook on the Physics and Chemistry of Rare Earth*; North-Holland, Amsterdam, 1979; Vol. 3.
(25) Henkelman, G.; Uberuaga, B. P.; Jónsson, H. A Climbing Image Nudged Elastic Band Method for Finding Saddle Points and Minimum Energy Paths. *The Journal of chemical physics* **2000**, *113* (22), 9901–9904.
(26) Bader, R. F. W. *Atoms in Molecules*; Wiley Online Library, 1990.
(27) Tang, Y.; Zhang, H.; Cui, L.; Ouyang, C.; Shi, S.; Tang, W.; Li, H.; Chen, L. Electronic States of Metal (Cu, Ag, Au) Atom on CeO2 (1 1 1) Surface: The Role of Local Structural Distortion. *Journal of Power Sources* **2012**, *197*, 28–37.
(28) Jansen, M.; Fischer, P. Eine Neue Darstellungsmethode Für Monoklines Silber (I, III) Oxid

(AgO), Einkristallzüchtung Und Röntgenstrukturanalyse. *Journal of the Less Common Metals* **1988**, *137* (1–2), 123–131.
(29) Meyer, B. K.; Polity, A.; Reppin, D.; Becker, M.; Hering, P.; Klar, P. J.; Sander, T.; Reindl, C.; Benz, J.; Eickhoff, M.; et al. Binary Copper Oxide Semiconductors: From Materials towards Devices. *physica status solidi (b)* **2012**, *249* (8), 1487–1509.
(30) Camellone, M. F.; Fabris, S. Reaction Mechanisms for the CO Oxidation on Au/CeO2 Catalysts: Activity of Substitutional Au3+/Au+ Cations and Deactivation of Supported Au+ Adatoms. *Journal of the American Chemical Society* **2009**, *131* (30), 10473–10483.
(31) Standke, B.; Jansen, M. Ag2O3, a Novel Binary Silver Oxide. *Angewandte Chemie International Edition in English* **1985**, *24* (2), 118–119.
(32) Zhang, C.; Michaelides, A.; King, D. A.; Jenkins, S. J. Structure of Gold Atoms on Stoichiometric and Defective Ceria Surfaces. *The Journal of chemical physics* **2008**, *129* (19), 194708.
(33) Jones, P. G.; Rumpel, H.; Schwarzmann, E.; Sheldrick, G. M. Gold (III) Chloride Oxide. *Acta Crystallographica Section B: Structural Crystallography and Crystal Chemistry* **1979**, *35* (10), 2380–2381.
(34) Meyer, B. K.; Polity, A.; Reppin, D.; Becker, M.; Hering, P.; Klar, P. J.; Sander, T.; Reindl, C.; Benz, J.; Eickhoff, M.; et al. Binary Copper Oxide Semiconductors: From Materials towards Devices. *physica status solidi (b)* **2012**, *249* (8), 1487–1509.
(35) Yang, Z.; He, B.; Lu, Z.; Hermansson, K. Physisorbed, Chemisorbed, and Oxidized CO on Highly Active Cu- CeO2 (111). *The Journal of Physical Chemistry C* **2010**, *114* (10), 4486–4494.
(36) Shapovalov, V.; Metiu, H. Catalysis by Doped Oxides: CO Oxidation by AuxCe1- XO2. *Journal of Catalysis* **2007**, *245* (1), 205–214.
(37) Ganduglia-Pirovano, M. V.; Da Silva, J. L. F.; Sauer, J. Density-Functional Calculations of the Structure of near-Surface Oxygen Vacancies and Electron Localization on CeO 2 (111). *Physical review letters* **2009**, *102* (2), 26101.
(38) Szabová, L.; Camellone, M. F.; Huang, M.; Matol\'\in, V.; Fabris, S. Thermodynamic, Electronic and Structural Properties of Cu/CeO 2 Surfaces and Interfaces from First-Principles DFT+ U Calculations. *The Journal of Chemical Physics* **2010**, *133* (23), 234705.
(39) Kim, H. Y.; Henkelman, G. CO Oxidation at the Interface between Doped CeO2 and Supported Au Nanoclusters. *The journal of physical chemistry letters* **2012**, *3* (16), 2194–2199.
(40) Garc\'\ia-Melchor, M.; López, N. Homolytic Products from Heterolytic Paths in H2 Dissociation on Metal Oxides: The Example of CeO2. *The Journal of Physical Chemistry C* **2014**, *118* (20), 10921–10926.
(41) Fernández-Torre, D.; Carrasco, J.; Ganduglia-Pirovano, M. V.; Pérez, R. Hydrogen Activation, Diffusion, and Clustering on CeO2 (111): A DFT+ U Study. *The Journal of chemical physics* **2014**, *141* (1), 14703.
(42) Capdevila-Cortada, M.; Łodziana, Z.; López, N. Performance of DFT+U Approaches in the Study of Catalytic Materials. *ACS Catalysis* **2016**, *6* (12), 8370–8379. https://doi.org/10.1021/acscatal.6b01907.
(43) Juarez, R.; Parker, S. F.; Concepcion, P.; Corma, A.; Garcia, H. Heterolytic and Heterotopic Dissociation of Hydrogen on Ceria-Supported Gold Nanoparticles. Combined Inelastic Neutron Scattering and FT-IR Spectroscopic Study on the Nature and Reactivity of Surface Hydrogen Species. *Chemical Science* **2010**, *1* (6), 731–738.

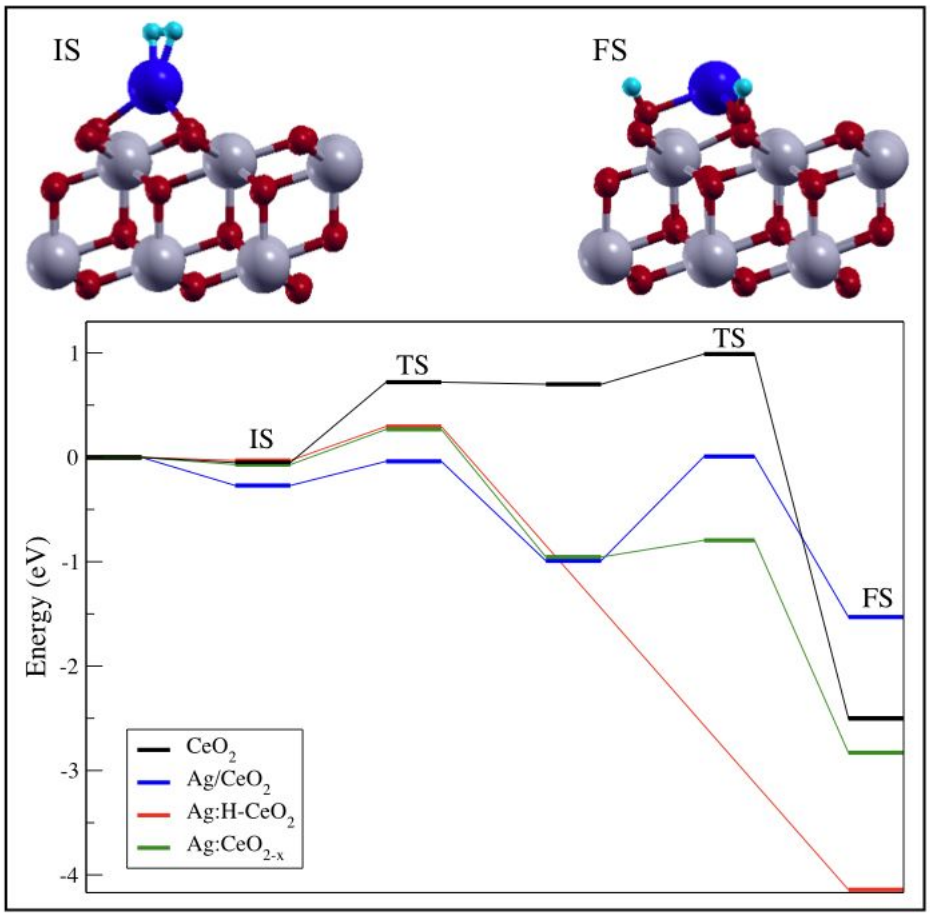

Figure Toc graphic